ELSEVIER
Available online at www.sciencedirect.com
ScienceDirect
Acta Materialia xxx (2008) xxx–xxx
Acta MATERIALIA
www.elsevier.com/locate/actamat

Inter-martensite strain evolution in NiMnGa single crystals

R.F. Hamilton [a], H. Sehitoglu [a,*], K. Aslantas [b], C. Efstathiou [a], H.J. Maier [c]

[a] Department of Mechanical Science and Engineering, University of Illinois at Urbana-Champaign, 1206 West Green Street, Champaign, IL 61821, USA
[b] Department of Mechanical Education, University of Afyon Kocatepe, A.N.S Campus, Afyon 03200, Turkey
[c] University of Paderborn, Lehrstuhl f. Werkstoffkunde, D-33095 Paderborn, Germany

Received 10 November 2007; received in revised form 7 January 2008; accepted 8 January 2008

UNCORRECTED PROOF

Abstract

Stress-induced martensitic transformations are clarified in classes of NiMnGa alloys which undergo the stress-free, thermal-induced inter-martensite transformation austenite (A) $\rightleftharpoons$ pre-martensite (PM) $\rightleftharpoons$ martensite. This study implements a comprehensive experimental approach, including analysis of the strain–temperature and stress–strain response, which discloses stress-induced inter-martensite transitions. The evolution of the transitions is elucidated using in situ digital image correlation (DIC) measurements of meso-scale strain fields. Under stress, this body of work unequivocally demonstrates that the transformation path becomes A $\rightleftharpoons$ PM $\rightleftharpoons$ I $\rightleftharpoons$ $10M$. The I-phase is an intermediate stress-induced martensite with a modulation period between three and five-layers. Owing to the intermediate transition, the thermal hysteresis in the strain–temperature response is tiny (<10 °C) compared with the hysteresis (32 °C) for A $\rightleftharpoons$ $10M$. The differential hysteresis levels are rationalized based on a thermo-mechanical formulation. Meso-scale DIC measurements quantify inter-martensite strain levels, which are indistinguishable from macro-scale stress–strain and strain–temperature responses.
© 2008 Acta Materialia Inc. Published by Elsevier Ltd. All rights reserved.

Keywords: Digital image correlation; Compression test; Strain vs. temperature; Thermal hysteresis; Metastable phases

1. Introduction

Shape memory alloys (SMA) undergo a reversible martensitic transformation (MT) during constant load temperature cycling and constant temperature load cycling. Classes of SMA designated ferromagnetic shape memory alloys (FSMA) exhibit magnetic field induced strains in the martensitic state. NiMnGa alloys are classes of FSMA that have attracted attention mainly due to promising magnetic field induced strains [1,2]. Reports on the stress–strain response at constant temperature show that these alloys recover strains above 10% and exhibit stress hysteresis from 10 to 100 MPa [3], making them good candidates for non-magnetic SMA applications. NiMnGa alloys with M_s temperatures near or below –73 °C undergo a thermal-induced transformation austenite (A) $\rightleftharpoons$ pre-martensite (PM) $\rightleftharpoons$ martensite (M) without stress [4]. Narrow thermal hysteresis has been reported for the initial transformation A $\rightleftharpoons$ PM (~3 °C) and the subsequent inter-martensitic transition PM $\rightleftharpoons$ $10M$ (~10 °C) [5,6]. The number of published reports on the transformation under stress and the accompanying hysteresis is insufficient [7–9]. Of these reports, only Kokorin et al. [7] consider constant load thermal cycling. The current work expounds on the stress-induced transformation using constant load thermal cycling at increasing compressive stress levels for the first time.

To characterize the PM phase, Zheludev et al. [10,11] study neutron scattering measurements of the $[\zeta\,\zeta\,0]$ TA_2 phonon dispersion curves. For the $10M$ structure, which exhibits five-layer modulation, the $\zeta = \zeta_M = 0.43$. They characterize the PM as a modulation of the austenite crystal structure ($L2_1$) with displacements along $(1\,\bar{1}\,0)$ that corresponds to $\zeta = \zeta_0 = 0.33$. Under stress, ζ_0 increases to 0.36 at 95 MPa [11]. From the work of Zheludev and his colleagues, we understand that the modulation of stress-induced intermediate martensite is sensitive to stress. More

Q1 * Corresponding author. Tel.: +1 217 333 4112; fax: +1 217 244 6534.
E-mail address: huseyin@uiuc.edu (H. Sehitoglu).

1359-6454/$34.00 © 2008 Acta Materialia Inc. Published by Elsevier Ltd. All rights reserved.
doi:10.1016/j.actamat.2008.01.007

UNCORRECTED PROOF

recently, the PM has been identified as three-layer modulated martensite [12]. This study investigates the alloy composition $Ni_{48.4}Mn_{27}Ga_{24.6}$, which undergoes the unstressed thermal-induced transformation $A \rightleftharpoons PM \rightleftharpoons 10M$. To elucidate the transformation path under stress, this work presents an original in situ digital image correlation (DIC) analysis of meso-scale transformation strains during load cycling at a constant temperature and constant load temperature cycling.

The transformation path during constant load temperature cycling is unclear in the literature for NiMnGa alloys that undergo the unstressed thermal-induced $A \rightleftharpoons PM \rightleftharpoons 10M$ transformation. Kim et al. [8] report the $A \rightleftharpoons PM \rightleftharpoons PM$ in [001] oriented single crystals; where the X-phase is a stress-induced intermediate phase of unknown crystal structure. Remarkably, they report the opposite inter-martensitic transition $PM \rightleftharpoons X$ for the stress–strain case and provide no explanation for the discrepancy. Kokorin et al. [7], in contrast, do not report an intermediate transition prior to the PM phase. They denote the pre-martensite phase I and report the transformation path $A \rightleftharpoons I \rightleftharpoons M$. The martensite (M) structure is not reported. From the authors' constant load temperature cycling study, it is unequivocally ascertained that the $A \rightleftharpoons PM \rightleftharpoons 10M$ transformation becomes $A \rightleftharpoons PM \rightleftharpoons I \rightleftharpoons 10M$ with increasing stress. Here, the I-phase is a stress-induced intermediate phase different from PM. From the findings of Zheludev and his colleagues, the modulation should be between three-layers and five-layers for the I-phase in the current $Ni_{48.4}Mn_{27}Ga_{24.6}$ alloy.

Unprecedented two-stage strain–temperature responses measured during constant load temperature cycling are presented. The first stage commences with the $A \rightleftharpoons PM$ transformation. Meso-scale in situ DIC strain measurements expose that the inter-martensitic transformation $PM \rightleftharpoons I$ transformation takes place as well. The second stage is attributed to $I \rightleftharpoons 10M$. The $A \rightleftharpoons PM \rightleftharpoons I$ transformation produces a thermal hysteresis ~1 °C and the $I \rightleftharpoons 10M$ transition results in a thermal hysteresis <10 °C. The narrow hysteresis is rationalized based on a thermo-mechanical formulation. In the stress–strain case, as the temperature is raised, the response changes from two stages (i.e., two plateau stresses) to a single stage. An outstanding finding from the in situ DIC technique is that the inter-martensitic transformation $A \rightleftharpoons I \rightleftharpoons 10M$ persists when a single plateau is observed. Ultimately, the results underscore that implementing in situ DIC to study the evolution of meso-scale strain fields in stress–strain and strain–temperature responses is a novel approach to investigating inter-martensitic phase transitions.

2. Material and experimental methods

The alloy was cast to the nominal composition $Ni_{48.4}Mn_{27.0}Ga_{24.6}$ (at.%). Single crystal ingots were grown using the Bridgman technique. Compression ($4 \times 4 \times 10$ mm^3) specimens were electro-discharge machined from the ingots such that loading is along the [001] orientation with the side faces parallel to the (100) plane. To characterize the unstressed MT, heat flow was measured as a function of temperature using a Perkin Elmer Pyris 1 differential scanning calorimeter (DSC). Two peaks were observed in the cooling (forward MT) and heating (reverse MT) thermo-grams. The first and second peaks start at −34 and −95 °C, respectively, and the corresponding thermal hysteresis are 5 and 15 °C. Furthermore, the latent heat of transformation for the second peak is twice that of the first. The larger transformation hysteresis and latent heat for the second peak are indicative of the MT. Transmission electron microscopy reveals that the predominant martensitic phase is $10M$. For the first peak, which exists at the higher temperature, a thermal-induced pre-martensitic transformation (PM) takes place. The PM is typically observed for NiMnGa alloys that undergo MTs below −73 °C [4]. Planes et al. [6] report differential hysteresis and latent heat measurements for the PM and MT comparable with those observed here. With this, the stress-free thermal-induced transformation is $A \rightleftharpoons PM \rightleftharpoons 10M$ in the current $Ni_{48.4}Mn_{27.0}Ga_{24.6}$ alloy.

Mechanical loading experiments were conducted on an Instron servo-hydraulic load frame. Isothermal load cycling experiments were conducted under position control. For temperature cycling, the specimens were enclosed in an insulated environment. The specimen was cooled and heated via conduction; the grips were cooled and heated using liquid nitrogen and an induction heater. A thermocouple was welded to the specimen to measure the temperature, and scan rates were approximately $\pm 10\ °C\ min^{-1}$. Macro-scale strain was measured with a miniature extensometer with a 3 mm gauge length. Within the gauge length, meso-scale strains were calculated using a full-field optical measurement technique called DIC. For DIC analysis, the specimen surface was polished and a speckle pattern was spray painted onto it. In situ images of the specimen surface were captured with an IMI model IMB–202FT (1600 × 1200 pixels) and Sony XCD-sx900 (1280 × 960 pixels) CCD cameras. Image acquisition was programmed into the mechanical testing software, which is based on National Instruments LabVIEW. Displacements were measured by tracking the evolution of the speckle pattern. The strains were calculated from the displacement gradients. Image correlation and subsequent strain calculations were achieved using software developed by Correlated Solutions (www.correlatedsolutions.com).

3. Experimental results

3.1. Compressive strain–temperature response

For constant stress–temperature cycling, compressive stress magnitudes are monotonically increased from 3 to 100 MPa. Representative strain–temperature (ε–T) responses are included in Fig. 1. At each stress level, the final martensite product is $10M$ structure based on TEM

Please cite this article in press as: Hamilton RF et al., Inter-martensite strain evolution in NiMnGa single crystals, Acta Mater (2008), doi:10.1016/j.actamat.2008.01.007

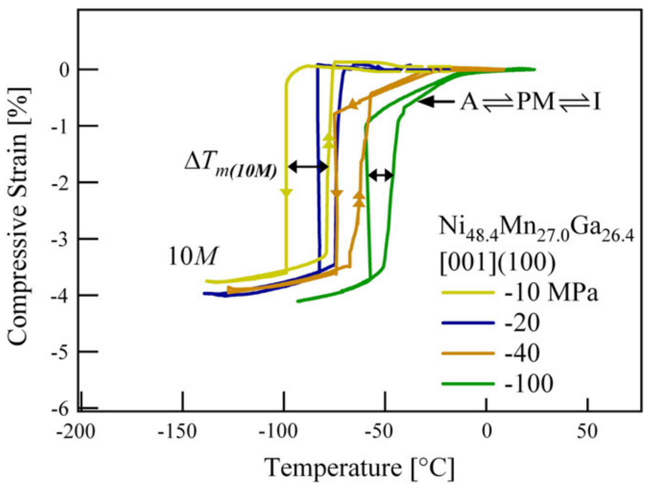

Fig. 1. Compressive strain–temperature responses. Single and double arrows mark cooling and heating curves, respectively. The 10*M* is the final martensite structure, and the corresponding thermal hysteresis is designated $\Delta T_{m(10M)}$. At −40 and −100 MPa, two stages are evident. In the first stage, the A denotes austenite, PM denotes pre-martensite, and I denotes an intermediate stress-induced phase.

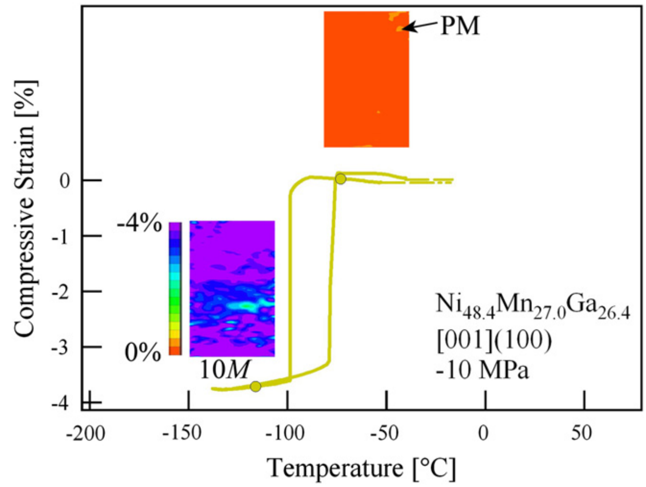

Fig. 2. Compressive strain–temperature response at −10 MPa. In situ strain fields are included, which are measured using DIC. Strain fields are reported during cooling, and circles along the cooling curve mark where the image is captured.

analysis. The cooling ε–T curve becomes vertical as the material transforms to the 10*M* structure. Specifically, the transition to the 10*M* structure starts and ends at the same temperature. Prior to the vertical segment, the curve is nonlinear at −10 MPa; however, there is a sharp corner at −20 MPa. It will be rationalized that this contrast marks a change in the transformation path.

At −40 to −100 MPa, the ε–T responses exhibit two different slopes, which evidence a two-stage transformation. The first stage starts at $M_s \approx -28$ °C. The temperature is close to the stress-free start temperature $M_{s(PM)} = -34$ °C, and thus, the A → PM commences. Note that the increase in M_s is expected owing to the application of stress. The first stage proceeds over a broad temperature range (∼50 °C), which is markedly different from the nearly isothermal second stage. To shed light on the transformation path for the two-stage case, the evolution of meso-scale strain fields is studied using in situ DIC.

3.2. In situ DIC: strain–temperature response

In situ DIC strain field measurements at −10 and −40 MPa are shown in the inset images in Figs. 2 and 3, respectively. Successive images are captured during cooling, and selected images are presented in the figures. In Fig. 2, the strain fields are shown for the ε–T response at −10 MPa. Within the initial image, the strain field is primarily 0%. An arrow points to a region of non-zero strain. Considering that the image is taken at −74 °C and this temperature is below the stress-free $M_{s(PM)} = -34$ °C, thermal-induced, self-accommodated groups of multiple PM variants can exist within the microstructure. The self-accommodated arrangement will inherently minimize strain energy and, thus, a nil strain field is evident in the initial image. A finite volume fraction of austenite remains untransformed with a null field as well, which will be explained on considering in situ DIC measurements at −40 MPa. The region of non-zero strain is attributed to the reorientation of a finite volume fraction of self-accommodated PM into a single variant. The mixture of austenite and PM converts to the 10*M* structure upon further cooling.

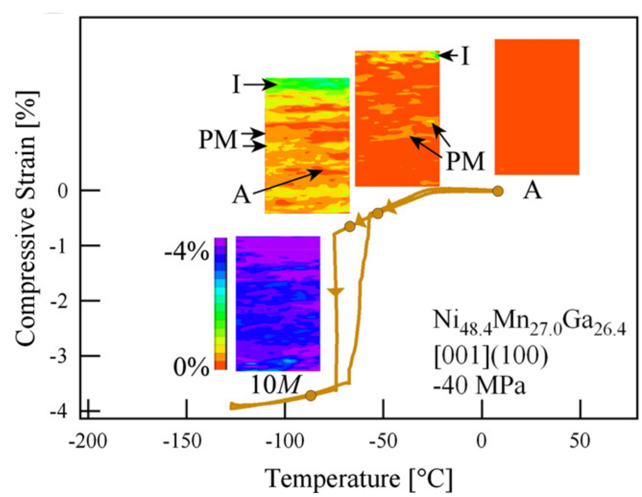

Fig. 3. Compressive strain–temperature response at −40 MPa showing illustrating the two-stage transformation path. In situ DIC strain fields show the meso-scale strain evolution throughout the first stage. In the text, the authors rationalize the nucleation of PM and the stress-induced I-phase prior to the transformation to 10*M*.

DIC strain field measurements at −40 MPa are shown in Fig. 3. The matrix is initially austenitic, i.e., zero strain field. Recall that the start temperature for the first stage implies that the A → PM transformation commences. From the second and third images, a larger volume fraction

Please cite this article in press as: Hamilton RF et al., Inter-martensite strain evolution in NiMnGa single crystals, Acta Mater (2008), doi:10.1016/j.actamat.2008.01.007

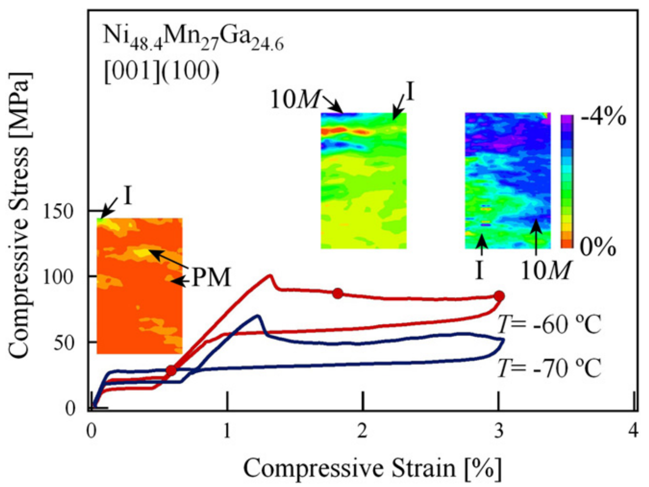

Fig. 4. Compressive stress–strain responses at −60 and −70 °C showing two stress plateaus, which evidence a two-stage transformation path. In situ DIC strain images are included at −60 °C. Based on the evolution of the meso-scale strain fields, the pre-existing, self-accommodated PM phase reorients and de-twins at the first stage. During the second stage, an intermediate martensite phase (I) is stress-induced from PM, which then converts to the 10M phase.

of PM phase reorients into a single variant, which most likely de-twins at the higher load. Also, null fields exist within the images. It is anticipated that these fields correspond to untransformed austenite that exists below $M_{f(PM)} \approx -39$ °C. Note that these null fields cannot correspond to self-accommodated PM. This is because at −40 MPa, self-accommodated PM would deform and produce measurable strain, as the stress level exceeds the maximum stress required to reorient and de-twin self-accommodated PM, which is approximately −30 MPa at −60 °C in Fig. 4. In Fig. 3, a conspicuous band appears near the top of the third image, in which strain levels approach −2%. In situ DIC for the stress–strain response will show that a stress-induced intermediate phase (I-phase) reaches a maximum strain of nearly −2%; hence, the green[1] band within the third image in Fig. 4 represents the I-phase. The PM phase reaches a maximum strain of −0.75% prior to converting to the I-phase. For regions of −0.75% strain (yellow contours), the PM phase exists. Therefore, the A ⇌ PM ⇌ I transformation is stress-induced in the first stage of the ε–T response. The second stage is attributed to I ⇌ 10M, and the strain is nearly −4%.

At −10 (Fig. 2) and −40 MPa (Fig. 3), the images for the 10M phase do not exhibit uniform strain fields. The heterogeneous local strain fields can imply multiple interface transformations. This finding is remarkable because the cooling ε–T curve is isothermal, which typically implies a single interface transformation in single crystals [13]. The isothermal transformation is rationalized in the discussion.

[1] For interpretation of color in Fig. 4, the reader is referred to the web version of this article.

3.3. In situ DIC: stress–strain response

Representative stress–strain (σ–ε) responses in the temperature (T) range $-70 \leqslant T \leqslant -50$ °C are shown in Fig. 4. This range is between the stress-free reverse transformation temperatures for PM ← 10M ($A_{f(10M)} \approx -80$ °C) and A ← PM ($A_{f(PM)} \approx -30$ °C) determined from the DSC analysis. Within this temperature range, the matrix will contain the PM phase. Recall that the in situ DIC study of the ε–T response (Fig. 3) revealed that a finite volume fraction of material will retain the untransformed austenite structure. Likewise, the matrix consists of austenite and self-accommodated PM in the range $-70 \leqslant T \leqslant -50$ °C. The σ–ε response at −60 °C exhibits two stress plateaus which are indicative of a two-stage transformation. Selected DIC strain-fields are shown during loading. Notice that the critical stress for the first stage decreases with increasing temperature. The opposite trend is expected for the first-order transition A ⇌ PM; therefore, the first stage is attributed to reorientation and de-twinning of pre-existing self-accommodated PM domains. Note that the maximum strain level is −0.75%, similar to the maximum level observed for the PM phase in the ε–T response. The strain fields within the second image (Fig. 4) exhibit striking contrasts and are predominantly −2%. Because the critical stress is exceeded prior to the drastic strain evolution, an intermediate (I-phase) is stress-induced. Through the plateau, the I-phase converts to 10M and the strain fields within final image evidence a mixture of the two phases. Notice that the I-phase began to nucleate in the first image. The same location in the second image exhibits strain fields that evidence the 10M phase. From this DIC analysis, one gleans that the first and second plateaus, respectively, manifest the A ⇌ PM and PM ⇌ I ⇌ 10M transformation paths in this $Ni_{48.4}Mn_{27}Ga_{24.6}$ alloy.

At $T > -50$ °C, the σ–ε curves exhibit a single plateau, which is demonstrated in Fig. 5. At these temperatures,

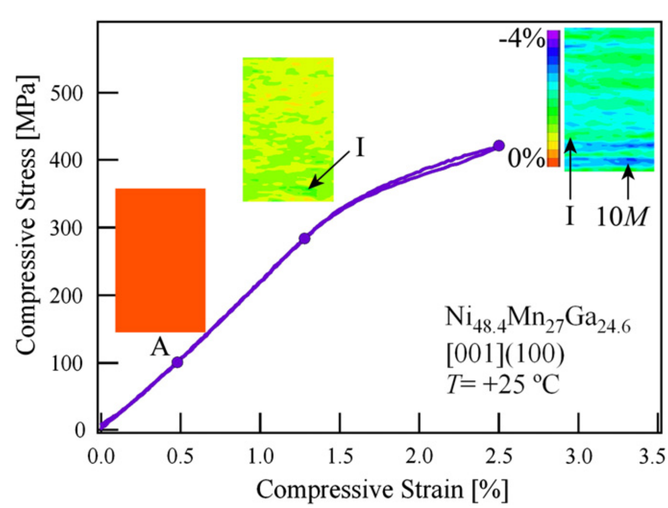

Fig. 5. Compressive stress–stain response at +25 °C showing a single stage. The evolution of meso-scale in situ DIC strain fields exposes that the inter-martensitic transformation A ⇌ I ⇌ 10M takes place.

UNCORRECTED PROOF

Please cite this article in press as: Hamilton RF et al., Inter-martensite strain evolution in NiMnGa single crystals, Acta Mater (2008), doi:10.1016/j.actamat.2008.01.007

the matrix will have a stabilized austenitic structure because they are much higher than the stress-free $A_{f(PM)} \approx -30\ ^{\circ}C$. To ensure DIC analysis is performed in the austenitic state, images are captured at $+25\ ^{\circ}C$. Indeed, the first image in Fig. 5 exhibits a homogeneous austenite structure based on the uniform zero strain field. Near the transformation stress -300 MPa (measured as the deviation from linearity), the I-phase begins to nucleate within the second image; an arrow marks a strain measurement that reaches -2%. Once the transformation stress is exceeded, the strain fields in the last image reflect that the I-phase is predominant. Furthermore, bands of $10M$ martensite form which achieve strain levels of -3.5%. The value exceeds the macro-scale strain measurement by 1%. The results show that the inter-martensitic transformation $A \rightleftharpoons I \rightleftharpoons 10M$ takes place despite the absence of multiple stress plateaus.

4. Discussion

For the $Ni_{48.4}Mn_{27}Ga_{24.6}$ alloy studied in this work, the stress-free thermal-induced transformation is $A \rightleftharpoons PM \rightleftharpoons 10M$. The PM is a micro-modulated phase with a $3M$ structure [5–7,11,12,14]. Zheludev et al. [10] and Planes et al. [5,6] envisage that PM and austenite can coexist after the initial transformation. The current in situ DIC analysis during thermal cycling at constant stress (Figs. 2 and 3) illustrates that this is indeed the case. and only a fraction of the austenite undergoes the $A \rightleftharpoons PM$. Based on this finding, the initial microstructure is composed of austenite and self-accommodated PM when the σ–ε responses exhibit two plateaus at temperatures between the stress-free A_f temperatures for $PM \leftarrow 10M$ and $A \leftarrow PM$ (Fig. 4). The two plateaus evidence a two-stage transformation. The initial stage is attributed to reorientation and de-twinning of pre-existing self-accommodated PM domains. Furthermore, the macro-scale strain levels achieved throughout the initial stage decrease with increasing temperature, because less self-accommodated PM exists at higher temperatures. From the evolution DIC strain fields, a stress-induced inter-martensitic transition $PM \rightarrow I$ is observed within the second stage at the highest critical stress (Fig. 4). The I-phase is a stress-induced intermediate phase, which transforms to $10M$ during the second stage. Using the in situ DIC technique, the authors have clarified the transformation path for two-stage σ–ε response. Specifically, contrary to Kim and his colleagues' [8] report that attributes the first stage to the stress inducement of an X-phase, the first stage corresponds to reorientation and de-twinning of PM. In the following, this original study of the strain–temperature (ε–T) response for this class of NiMnGa alloys is discussed.

The ε–T response changes from one ($A \rightleftharpoons 10M$) to two ($A \rightleftharpoons PM \rightleftharpoons I$ and $I \rightleftharpoons 10M$) stages with increasing stress (Fig. 1). At each stress level, the forward transformation to the $10M$ starts and ends at the same temperature, and thus the transformation is isothermal. The temperature interval during the forward MT is related to stored elastic strain energy; a wide interval implies more energy is stored [13,15]. As a single interface propagates in single crystalline alloys, no constraint is imposed on interface motion by grain boundaries or neighboring martensite variants. Therefore, the shape change takes place freely as the single interface traverses the single crystal, and no elastic strain energy is stored [13,15]. For the $Ni_{48.4}Mn_{27}Ga_{24.6}$ alloy, however, DIC strain images captured at the end of the isothermal cooling ε–T segment (Figs. 2 and 3) suggest that multiple interfaces can exist. If a single interface had traversed the imaged area, a homogeneous strain field should exist [16]. Because this is not the case, the strain fields in Figs. 2 and 3 most likely indicate that multiple interfaces exist. Apparently, the habit plane, the undistorted plane between the I and $10M$ phases, must be created easily, and thus, the level of stored strain energy is inconsequential. To the contrary, substantial strain energy is stored for the first transformation ($A \rightleftharpoons PM$) in the two-stage ε–T responses (-40 and -100 MPa). This is based on the wide transformation temperature range ($\sim 50\ ^{\circ}C$). Strain energy storage is significant because it builds up by contributions from both the $A \rightleftharpoons PM$ and $PM \rightleftharpoons I$ transformations (Fig. 3).

For the $A \rightleftharpoons PM \rightleftharpoons I$ inter-martensitic transformation, the heating and cooling ε–T curves overlap at -40 MPa and a tiny thermal hysteresis ($<1\ ^{\circ}C$) exists. At -100 MPa (Fig. 1), though the ε–T curves do not overlap, the thermal hysteresis is still small; the hysteresis measured A_f–M_s is $<1\ ^{\circ}C$. Furthermore, the transition to the $10M$ exhibits a smaller hysteresis when it is stress-induced from the I-phase at compressive stress magnitudes -40 and -100 MPa (Fig. 1); the thermal hysteresis $\Delta T_{m(10M)} \approx 12\ ^{\circ}C$ is narrower than that measured at -10 MPa ($\Delta T_{m(10M)} = 21\ ^{\circ}C$). The differential hysteresis levels are rationalized in the following based on a thermo-mechanical formulation outlined in previous work [17,18].

An expression for the thermal hysteresis has been derived [18]:

$$\Delta T_h = A_f - M_s = (F_{C(R)} + F_{C(F)})/|\Delta s|$$

$F_{C(R)}$ and $F_{C(F)}$, respectively, represent the dissipative potential for the reverse and forward transformation [17]. F_C is related to the frictional work that must be overcome for interfacial motion [19]. $|\Delta s|$ is the magnitude of the entropy change for the MT and $\Delta s = Q/T_0$, where the latent heat Q equals the area under a DSC peak divided by the temperature scan rate. The equilibrium temperature T_0 is estimated as half the sum of the cool and heat peak temperatures. A small change implies a small F_C, and thus will facilitate a narrow hysteresis and vice versa. For the pre-martensite and $10M$ phases, respectively, the $|\Delta s| = 0.0034$ and $0.0138\ J\ (g\ ^{\circ}C)^{-1}$. Based on this result, the $A \rightleftharpoons PM$ facilitates the narrow thermal hysteresis for the first stage.

The hysteresis for the transition to $10M$ becomes narrow for the two-stage transformation compared with the $A \rightleftharpoons 10M$ (compare -10 and -40 MPa in Fig. 1). In this case,

UNCORRECTED PROOF

Please cite this article in press as: Hamilton RF et al., Inter-martensite strain evolution in NiMnGa single crystals, Acta Mater (2008), doi:10.1016/j.actamat.2008.01.007

the forward and reverse transformations correspond to $I \rightleftharpoons 10M$. The $|\Delta s|$ for this transformation is likely lower than that for $A \rightleftharpoons 10M$; considering that, the habit plane between I and $10M$ the phases should be created easily. Moreover, because the I-phase is stress-induced, it will be unstable and $I \rightleftharpoons 10M$ will experience a lower F_C. These two factors promote the shrinking hysteresis $\Delta T_{m(10M)}$ in Fig. 1. In addition, the elastic strain energy stored during the $A \rightleftharpoons PM \rightleftharpoons I$ transformation facilitates the smaller hysteresis. The energy assists the reverse transformation enabling it to start closer to A_f (compare Figs. 2 and 3) [17]. Remarkably, for the ε–T response at -20 MPa (Fig. 1) the hysteresis is the smallest $\Delta T_{m(10M)} = 8.5$ °C. Based on the narrow hysteresis, the $A \rightleftharpoons PM \rightleftharpoons I$ may be facilitated initially, despite the absence of multiple stages. Note that this is substantiated by the abrupt start to the MT, which matches that observed at -40 MPa

5. Conclusions

This work has presented a study of the thermal- and stress-induced MT in [0 0 1] oriented $Ni_{48.4}Mn_{27}Ga_{24.6}$ single crystals. The thermal-induced transformation path is austenite(A) $\rightleftharpoons$ pre-martensite(PM) $\rightleftharpoons 10M$. Under stress, however, the $10M$ structure is stress-induced from the PM via an intermediate MT, and thus, the inter-martensitic transformation path is $A \rightleftharpoons PM \rightleftharpoons I \rightleftharpoons 10M$. The I-phase is a modulated phase with a period between that of the three-layer PM phase and the five-layer $10M$ phase based on previous investigations. From a comprehensive study, including in situ DIC measurements of the meso-scale full-field transformation strains during thermal cycling under load, i.e., strain–temperature response, and during isothermal load cycling, i.e., stress–strain, the following conclusions are made:

1. The stress-free thermal-induced $A \rightleftharpoons PM$ transformation is localized. This is not immediately evident based on DSC analysis, in which two separate peaks exist, which can imply $A \rightleftharpoons PM$ and a subsequent $PM \rightleftharpoons 10M$ inter-martensitic transformation. From in situ DIC during thermal cycling under low constant compressive stress demonstrates, the transformation is more likely $A \rightleftharpoons A + PM$, with austenite being the predominant structure, followed by $A + PM \rightleftharpoons 10M$. From in situ DIC during thermal cycling under constant compressive stress, we ascertain that a finite volume fraction of austenite remains untransformed below M_f for the first DSC peak. This demonstrates that the initial transformation is more likely $A \rightleftharpoons A + PM$.
2. The transformation path at low constant stress levels is primarily $A \rightleftharpoons 10M$. At higher levels of constant stress, the path changes; two stages exist in the strain–temperature response. Based on findings from DIC analysis, the initial stage corresponds to $A \rightleftharpoons PM \rightleftharpoons I$ and the $I \rightleftharpoons 10M$ inter-martensitic transformation takes place throughout the second stage.
3. The inter-martensitic transformation $A \rightleftharpoons PM \rightleftharpoons I$ enhances elastic strain energy storage and curtails energy dissipation in the strain–temperature response. Consequently, the transformation path $A \rightleftharpoons PM \rightleftharpoons I \rightleftharpoons 10M$ exhibits a smaller thermal hysteresis compared with that for the predominantly $A \rightleftharpoons 10M$ MT.
4. For the stress–strain response, two stages develop. In situ DIC analysis reveals that the first and second stages correspond to reorientation and de-twinning of PM and a subsequent $PM \rightleftharpoons I \rightleftharpoons 10M$ inter-martensitic transformation.
5. The inter-martensitic transition $A \rightleftharpoons I \rightleftharpoons 10M$ takes place up to the highest compressive transformation stress levels. The transformation path is unequivocally confirmed from the in situ DIC strain fields, as the stress–strain response exhibits a single stage.
6. The PM, stress-induced I-phase and $10M$ martensite exhibit maximum strains of -0.75%, -2% and -4%, respectively.

Acknowledgements

The work was supported by the NSF Grant No. CMS-0428428. The single crystals were obtained from Prof. Y. Chumlyakov of Tomsk State University.

References

[1] Heczko O. J Magn Magn Mater 2005;290–291(PART 2):787.
[2] Callaway JD, Sehitoglu H, Hamilton RF, Aslantas K, Miller N, Maier HJ, et al. Appl Phys Lett 2006;89:221905.
[3] Martynov VV, Kokorin VV. J Phys III (Appl Phys, Mater Sci, Fluids, Plasma Instr) 1992;2:739.
[4] Chernenko VA, Segui C, Cesari E, Pons J. Phys Rev B Condens Mat 1998;57:2659.
[5] Perez-Reche FJ, Vives E, Manosa L, Planes A. Mater Sci Eng A 2004;378:353.
[6] Planes A, Obrado E, Gonzalez-Comas A, Manosa L. Phys Rev Lett 1997;79:3926.
[7] Kokorin VV, Chernenko VA, Cesari E, Pons J, Segui C. J Phys Condens Mat 1996;8:6457.
[8] Kim J-H, Fukuda T, Kakeshita T. Scripta Mater 2006;54:585.
[9] Karaca HE, Karaman I, Basaran B, Lagoudas DC, Chumlyakov YI, Maier HJ. Acta Mater 2007;55:4253.
[10] Zheludev A, Shapiro SM, Wochner P, Schwartz A, Wall M, Tanner LE. Phys Rev B Condens Mat 1995;51:11310.
[11] Zheludev A, Shapiro SM. Solid State Commun 1996;98:35.
[12] Brown PJ, Crangle J, Kanomata T, Matsumoto M, Neumann KU, Ouladdiaf B, et al. J Phys Condens Mat 2002;14:10159.
[13] Salzbrenner RJ, Cohen M. Acta Metall 1979;27:739.
[14] Zheludev A, Shapiro SM, Wochner P, Tanner LE. Phys Rev B Condens Mat 1996;54:15045.
[15] Ortin J, Planes A. Acta Metall 1988;36:1873.
[16] Efstathiou C, Sehitoglu H, Carrol J, Lambros J, Maier HJ. Acta Mater (submitted for publication). Q3
[17] Hamilton RF, Sehitoglu H, Chumlyakov Y, Maier HJ. Acta Mater 2004;52:3383.
[18] Hamilton RF, Sehitoglu H, Efstathiou C, Maier HJ. Acta Mater 2007;55:4867.
[19] Olson GB, Cohen M. Scripta Metall 1977;11:345.

UNCORRECTED PROOF